Interface Trap States in Al_2O_3/AlGaN/GaN Structure Induced by ICP Etching of AlGaN Surfaces

Zenji Yatabe [*,1,2], Joel T. Asubar[1,2], Taketomo Sato[1], and Tamotsu Hashizume[1,2]**

[1] Graduate School of Information and Science Technology and Research Center for Integrated Quantum Electronics (RCIQE), Hokkaido University, Sapporo 060-8628, Japan
[2] Japan Science and Technology Agency (JST), CREST, Chiyoda, Tokyo 102-0075, Japan

Received ZZZ, revised ZZZ, accepted ZZZ
Published online ZZZ (Dates will be provided by the publisher.)

Keywords MIS HEMTs, dry etching damage, interface state density

* Corresponding author: e-mail zenji.yatabe@rciqe.hokudai.ac.jp, Phone: +81 11 706 7176, Fax: +81 11 716 6004
** e-mail hashi@rciqe.hokudai.ac.jp, Phone: +81 11 706 7171, Fax: +81 11 716 6004

We have investigated the effects of the inductively coupled plasma (ICP) etching of AlGaN surface on the resulting interface properties of the Al_2O_3/AlGaN/GaN structures. The experimentally measured capacitance-voltage (*C-V*) characteristics were compared with those calculated taking into account the interface states density at the Al_2O_3/AlGaN interface. As a complementary method, photoassisted *C-V* method utilizing photons with energies less than the bandgap of GaN was also used to probe the interface state density located near AlGaN midgap. It was found that the ICP etching of the AlGaN surface significantly increased the interface state density at the Al_2O_3/AlGaN interface. It is likely that ICP etching induced the interface roughness, disorder of chemical bonds and formation of various type of defect complexes including nitrogen-vacancy-related defects at the AlGaN surface, leading to poor *C-V* curve due to higher interface state density at the Al_2O_3/AlGaN interface.

1 Introduction The combination of excellent intrinsic properties such as high breakdown field strength, high electron carrier velocity and high sheet carrier density has made GaN-based high-electron-mobility transistors (HEMTs) primary candidates for realizing ultra-low-loss power switching devices [1-6]. However, conventional AlGaN/GaN HEMTs with Schottky-gates are normally-on devices requiring a negative gate voltage to turn them off. For failure protection and reduced power consumption, normally-off operation is highly desirable. Normally-off operation also entails driving the gate with positive voltage to turn on the device which leads to large leakage current. To achieve simultaneously normally-off operation and gate leakage suppression, a combination of recessed and insulated gates structures is often used. Since the interface quality significantly affects the transistor performance, plasma-assisted dry etching to form the recessed gate region and the subsequent formation of an insulator-semiconductor interface are critical steps for fabricating such devices. It has been reported that plasma-assisted etching degrades the electrical and optical properties of GaN and AlGaN surfaces [7-10]. Tang et al. [11] examined the SiO_2/n-GaN-based capacitors and field-effect transistors (FETs) fabricated on a Cl_2-based inductively coupled plasma (ICP)-etched GaN surface. It was observed that ICP etching increased the interface state density $D_{it}(E)$ and degraded the field-effect mobility of the FET channel. To improve device performance and stability of metal-insulator-semiconductor (MIS) HEMTs using AlGaN/GaN structures, evaluation of electronic state properties of the interfaces between insulators and AlGaN is of utmost importance. Since trap states at the oxide-semiconductor interfaces may cause various operational stability and reliability issues in AlGaN/GaN-based MOS-HEMTs, low $D_{it}(E)$ at the insulator/AlGaN-based materials interfaces is highly imperative.

To investigate interface properties of Al_2O_3-insulated gates on AlGaN/GaN structures with and without (w/o) ICP etching of AlGaN surface, in this paper, we compared the measured capacitance-voltage (*C-V*) characteristics with those calculated, considering interface states density D_{it} (*E*) at the Al_2O_3/AlGaN interface. As a complementary

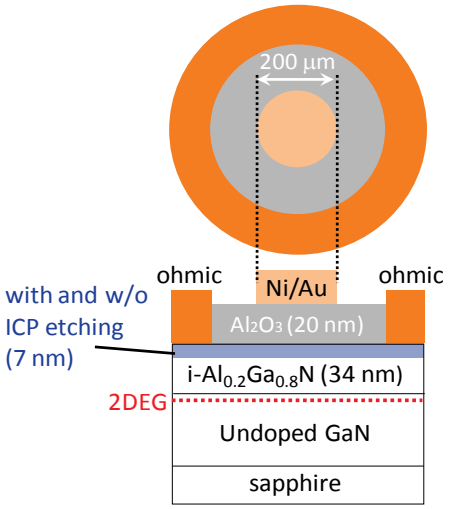

Figure 1 Schematic illustration of the $Al_2O_3/Al_{0.2}Ga_{0.8}N/GaN$ structure used in this study.

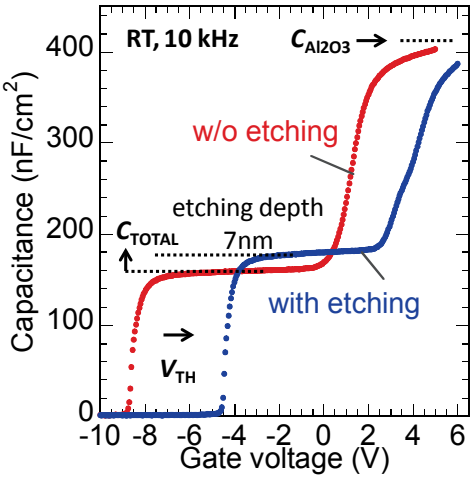

Figure 2 RT *C-V* characteristics of $Al_2O_3/Al_{0.2}Ga_{0.8}N/GaN$ structures with and without ICP etching.

method, photoassisted *C-V* method utilizing photons with energies less than the bandgap of GaN was also used to probe the $D_{it}(E)$ located near the midgap of the AlGaN.

2 Experimental Figure 1 shows a schematic illustration of the HEMT MIS structure used in this study. An undoped $Al_{0.2}Ga_{0.8}N/GaN$ heterostructure with an AlGaN layer thickness of 34 nm grown on a sapphire substrate by metal organic chemical vapor deposition (MOCVD) was used as the starting wafer (provided by NTT-AT). The sheet resistance and mobility of the AlGaN/GaN heterostructure were 500 Ω/sq. and 1750 $cm^2V^{-1}s^{-1}$, respectively. Two sets of Al_2O_3/AlGaN/GaN samples, i.e., (1) with and (2) without dry etching (control sample) of the AlGaN surface were then prepared. For etching the AlGaN surface, we used a Cl_2-based dry etching process assisted by ICP at RT. The ICP and bias power values were 300 and 5 W, respectively. The resulting etching depth was 7 nm as revealed by TEM investigations [12]. We then deposited a 10-nm-thick SiN_x film as a surface protection layer to avoid damage to the AlGaN surface during ohmic annealing [13]. As an ohmic electrode, a ring-shaped Ti/Al/Ti/Au multilayer structure was deposited on the AlGaN surface, followed by annealing at 800 ºC for 1 min in N_2 ambient. After the ohmic electrode formation, the SiN_x layer was removed in a buffered HF solution. An Al_2O_3 layer with a nominal thickness of 20 nm was then deposited at a deposition rate of 0.11 nm/cycle on the AlGaN surface using an atomic layer deposition system (ALD) (SUGA-SAL1500) at 350 ºC for 170 cycles. Trimethylaluminum (TMA) as the aluminium precursor and water vapor as the oxygen source were introduced into an ALD reactor in alternate pulse forms. Finally, a circular Ni/Au (20/50 nm) gate electrode concentric with the ohmic electrode as illustrated in Fig. 1 was deposited on the Al_2O_3 layer.

3 Results and Discussion We initially performed a conventional *C-V* measurement using an HP4192 impedance analyzer at a measurement frequency of 10 kHz at room temperature (RT) to characterize the Al_2O_3/AlGaN interface properties. Figure 2 compares the typical *C-V* characteristics of the Al_2O_3/AlGaN/GaN structures with and without the ICP etching of the AlGaN surface. Both samples showed *C-V* curves with two steps, peculiar to the MIS sample fabricated on the heterostructure including a two-dimensional electron gas (2DEG) [14-17]. The constant capacitance plateau at the forward bias corresponds to the Al_2O_3 oxide capacitance (C_{Al2O3}), whereas that at the reverse bias is that of the total capacitance consisting of Al_2O_3 and AlGaN layers (C_{TOTAL}). At the deep reverse bias, the capacitance steeply decreases to nearly zero, indicating the 2DEG depletion at the AlGaN/GaN interface.

For the ICP etched sample, we observed a shallower threshold voltage (V_{TH}) corresponding to 2DEG depletion. The increase in C_{TOTAL} (ΔC_{TOTAL}) can be accurately accounted for by the resulting etching depth of AlGaN (7 nm) layer. However, the ICP-etched sample showed a less steep slope of the *C-V* curve and a high on-set voltage at the forward bias regime. At the forward bias regime, acceptor-type interface states near the conduction band minimum can trap electrons and produce negative charges. Such ionization of acceptor-type states can screen the applied gate electric field, impeding the potential modulation of the AlGaN surface. The relatively slower increase in capacitance with increasing forward bias voltage suggests the presence of higher state densities at the Al_2O_3/ICP-etched AlGaN interface. It is also likely that the high-density interface states affect the V_{TH}. The V_{TH} difference (ΔV_{TH}) between the samples with and without the ICP etching was 4.1 V, as shown Fig. 2. Using the band offsets between Al_2O_3/AlGaN and AlGaN/GaN interfaces, the 2DEG den-

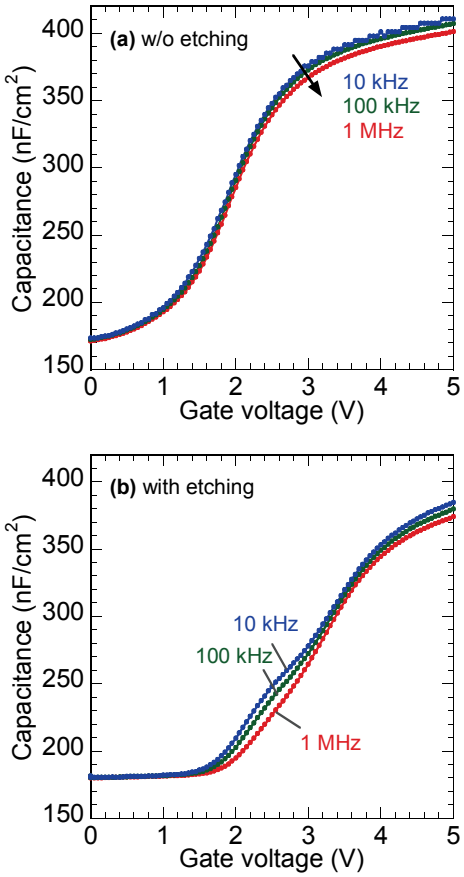

Figure 3 Frequency dispersion of the *C-V* curves of the $Al_2O_3/Al_{0.2}Ga_{0.8}N/GaN$ structures (a) without and (b) with ICP etching in the forward bias range at RT.

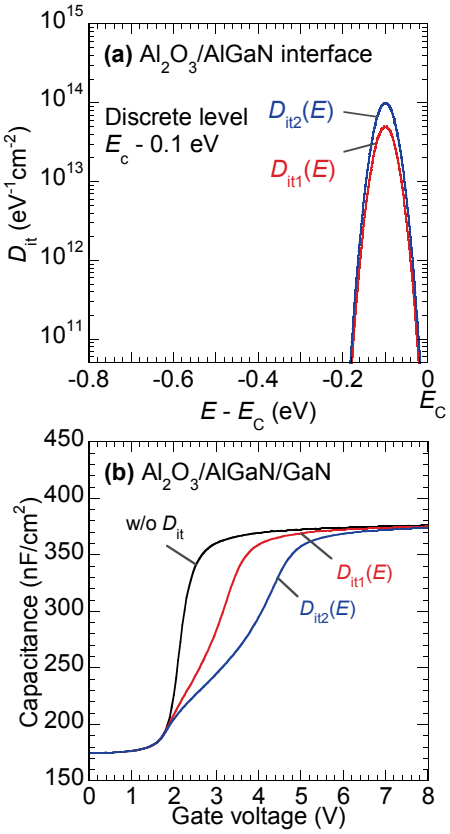

Figure 4 (a) Interface state density distribution used in calculation and (b) the calculated *C-V* curves of the $Al_2O_3/AlGaN/GaN$ structures considering (colored curves) and without considering (black curve) interface states.

sity n_s and C_{TOTAL}, it is straightforward to estimate ΔV_{TH}. *C-V* analysis using the Schottky contacts indicated that n_s decreased from 9.0×10^{12} to 7.0×10^{12} cm^{-2} after the ICP etching [12]. Correspondingly, ΔV_{TH} was calculated to be 3.0 V, smaller than the experimentally observed value. For the ICP-etched sample, it is expected that the high-density negative charges due to acceptor-type states shift the V_{TH} toward the positive voltage direction, which can explain the discrepancy between the experimental and the calculated ΔV_{TH} values.

Figure 3 (a) and (b) shows the frequency dispersion of the *C-V* characteristic with and without the ICP etching of the AlGaN surface at RT. For the ICP-etched sample, we clearly observed frequency dispersion and a distinct inflection point in the positive bias range possibly due to a discrete trap level at the Al_2O_3/AlGaN interface introduce by ICP etching. This could be connected to the increased density of nitrogen-vacancy (V_N)-related deep level defects induced by Cl_2-based ICP etching similar to those reported by Fang et al. regarding the GaN surface [18].

To shed a light on the origin of the observed inflection point in the *C-V* behavior, we then carried out calculations using a numerical solver of the Poisson equation based on the one-dimensional Gummel algorithm, taking into account the fixed charges at the AlGaN/GaN interface originating from spontaneous and piezoelectric polarization as well as the charge in the electronic states at the Al_2O_3/AlGaN interface [19-21]. Figure 4(a) shows the discrete interface state density distributions $D_{it}(E)$, which is Gaussian curve describing defect discrete states and the peak positions are E_C - 0.1 eV, used in calculation. The sheet densities corresponding to $D_{it1}(E)$ and $D_{it2}(E)$ are 2.7×10^{12} and 5.3×10^{12} cm^{-2}. The calculated *C-V* curves are shown in Fig. 4(b). In the forward bias region, we clearly reproduced the inflection point, similar to those experimentally observed from the etched samples.

By rigorous numerical fitting of experimental *C-V* curves with the analytical model, we have attempted to estimate the state density distribution in the Al_2O_3/AlGaN interfaces. Figure 5(a) shows the comparison between the calculated and experimental *C-V* curves of the $Al_2O_3/AlGaN/GaN$ structure with and without the ICP dry etching of the AlGaN surface. The initial HEMT structure has a 34-nm-thick AlGaN layer. After the ICP etching, the AlGaN thickness was reduced to 27 nm, causing an increase in C_{TOTAL} and a pronounced V_{th} shift in the *C-V* curve [12]. From the calculated *C-V* curves that best fit the

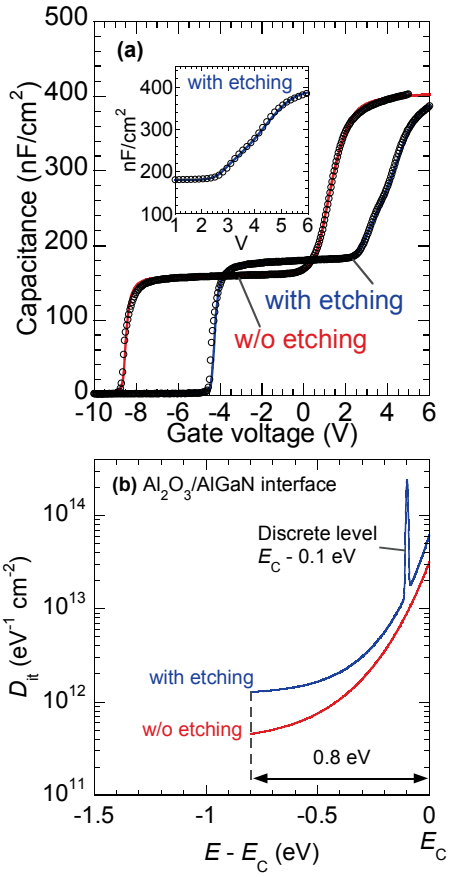

Figure 5 (a) Comparison between the calculated and experimental *C-V* curves of the Al_2O_3/AlGaN/GaN structure with and without the ICP etching of the AlGaN surface. By assuming interface state density distributions indicated by the solid lines in (b), the calculation reasonably reproduced the experimental data.

corresponding measured experimental *C-V* curves, we obtained interface state distribution given in Fig. 5b. For the ICP etched sample, a discrete level at (E_C - 0.1) eV was extracted from the calculated *C-V* curve that best fit the measured experimental *C-V* curve. From deep level transient spectroscopy measurements, Fang et al. [18] reported that several kinds of deep levels originating from defect complexes related to nitrogen vacancy can be increased at the GaN surface after Cl_2-based ICP etching. In particular, they attributed a deep center located at (E_C - 0.17) eV to V_N-related defect due to ICP etching. We believe that this is in reasonable agreement with our present results. It should also be mentioned that in this present work, we only assumed a single discrete state because it is enough to obtain a very good agreement between the calculated and measured *C-V* curves for the ICP etched sample. Considering the current samples under study, therefore, we believe that this discrete state is the highly dominant if not the only one present. However, we also believe that it is not remote to have other additional discrete states. Note that only the

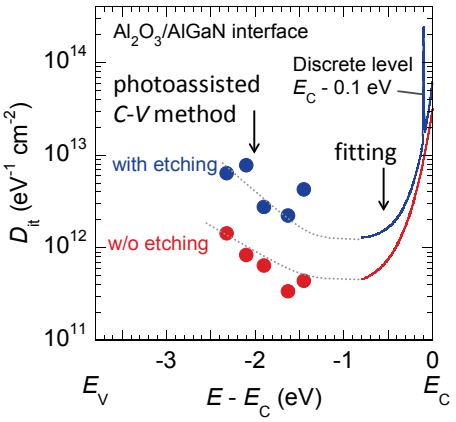

Figure 6 Interface state density distributions at the Al_2O_3/AlGaN interface determined by a combination of the photoassisted *C-V* method and the *C-V* fitting method.

interface states located from conduction band edge E_C to approximately E_C - 0.8 eV can effectively emit electrons at RT [19, 20]. At the step in the reverse bias regime, we observed similar *C-V* slopes for both samples. In this bias region, the Fermi level is located far below the valence band maximum of AlGaN at the Al_2O_3/AlGaN interface, making electron occupation probability of interface states no longer a function of the gate voltage [14, 19]. In addition, the electrons captured at deep interface states remain almost unchanged at RT even when a large negative bias is applied to the gate electrode, because the relatively deeper states have an extremely large time constant for electron emission to the conduction band [14].The interface states under this condition, therefore, act as fixed and frozen charges, rendering the detection of interface states by conventional *C-V* measurements at RT difficult. Consequently, we can only determine the state density distribution near E_C at the Al_2O_3/AlGaN interface from the fitting results.

To circumvent this problem, photoassisted *C-V* measurements similar to those described in Refs. 12 and 14 were performed to evaluate near-midgap interface states. Figure 6 shows the state density distributions at the Al_2O_3/AlGaN interface determined by the photoassisted *C-V* and the fitting methods. The sample without the ICP etching of the AlGaN surface showed state densities of at most around 1×10^{12} $cm^{-2}eV^{-1}$ or less near the midgap. On the other hand, much higher state densities were obtained from the Al_2O_3/ ICP-etched AlGaN interface. It should be mentioned that traps with associated time constants in the insulator and the AlGaN barrier layer could also result into frequency dispersion. To identify the presence of considerable amount of traps in the AlGaN barrier layer, we performed photoassisted *C-V* measurements on a Schottky-gated structure. Consequently, we observed no shift in the onset voltage of the Schottky-gated structure, suggesting negligible amount of deep level traps in the AlGaN layer.

For the traps in the insulator layer, it is rather difficult to quantify at this point. Nevertheless, we believe that interface states are the most dominant cause of frequency dispersion as explicitly stated in Ref. [22] and mathematically described in Ref. [23].

Transmission electron microscope observations have established that the ICP etching process can introduce a monolayer-level crystalline roughness to the AlGaN surface [12]. As a result, lattice disorder and/or a high density of dangling bonds near step edges remained at the AlGaN surface, leading to the generation of high-density electronic states with a continuous energy distribution [21]. From the Cl_2/BCl gas mixture used during the ICP etching, active Cl-based radicals dominantly react with the AlGaN surfaces to form volatile products, such as $GaCl_3$ and $AlCl_3$. In addition, there are also other possible chemical reactions. For instance, a highly volatile NCl_3 can be formed by a reaction between the Cl-based radical and N atoms, causing a preferential loss of N atoms at the AlGaN surface [24]. In fact, Fang et al. [18] reported that several kinds of deep levels originating from defect complexes related to nitrogen vacancy were increased at the GaN surface after the Cl_2-based ICP etching. It is thus likely that ICP etching leads to monolayer-level interface roughness, disorder of the chemical bonds and formation of various types of defect complexes at the AlGaN surface, resulting to poor *C-V* characteristics due to high-density interface states at the Al_2O_3/AlGaN interface.

4 Conclusion We have presented the results of our investigation of the effects of the Cl_2-based ICP etching of AlGaN surface on the interface properties of the Al_2O_3/AlGaN/GaN structures. Capacitance-voltage analyses at RT showed a two-step behavior, peculiar to a heterostructure MOS sample. We presented a calculation method of *C-V* characteristics for the HEMT MIS structures for evaluating the electronic state properties at the insulator/AlGaN interfaces. A comparison between experimental and simulation results showed that only a limited energy region of interface states is detectable using the conventional *C-V* analysis at RT. To facilitate evaluation of near-midgap electronic states at the insulator/AlGaN interfaces under RT, we have developed a photoassisted *C-V* method using monochromatic light with energy less than the GaN bandgap. It was found that the ICP etching of the AlGaN surface significantly increased the interface state density at the Al_2O_3/AlGaN interface. It is likely that ICP etching induced interface roughness, disorder of chemical bonds and formation of various type of defect complexes including V_N at the AlGaN surface, leading to poor *C-V* curve due to higher interface state density at the Al_2O_3/ICP-etched AlGaN interface. We believe that further investigation on interface states is absolutely necessary for achieving improved operation stability of AlGaN/GaN MIS HEMTs.

References

[1] M. Ishida, T. Ueda, T. Tanaka, and D. Ueda, IEEE Trans. Electron Dev. **60**, 3053 (2013).

[2] M. Van Hove, X. Kang, S. Stoffels, D. Wellekens, N. Ronchi, R. Venegas, K. Geens, and S. Decoutere, IEEE Trans. Electron Dev. **60**, 3071 (2013).

[3] T. Kikkawa, T. Hosoda, S. Akiyama, Y. Kotani, T. Wakabayashi, T. Ogino, K. Imanishi, A. Mochizuki, K. Itabashi, K. Shono, Y. Asai, K. Joshin, T. Ohki, M. Kanamura, M. Nishimori, T. Imada, J. Kotani, A. Yamada, N. Nakamura, T. Hirose, and K. Watanabe, Proc. 1st IEEE Workshop Wide Bandgap Power Devices and Application (WiPDA-2013), 2013, p. 11.

[4] B. Hughes, R. Chu, J. Lazar, S. Hulsey, A. Carrido, D. Zehnder, M. Musni, and K. Boutros, Proc. 1st IEEE Workshop Wide Bandgap Power Devices and Application (WiPDA-2013), 2013, p. 76.

[5] Y.-F. Wu, J. Gritters, L. Shen, R. P. Smith, J. McKay, and R. Birkhahn, Proc. 1st IEEE Workshop Wide Bandgap Power Devices and Application (WiPDA-2013), 2013, p. 6.

[6] N. Herbecq, I. Roch-Jeune, N. Rolland, D. Visalli, J. Derluyn, S. Degroote, M. Germain, and F. Medjdoub, Appl. Phys. Express **7**, 034103 (2014).

[7] J. Kuzmík, P. Javorka, M. Marso, and P. Kordos, Semicond. Sci. Technol. **17**, L76 (2002).

[8] K.-J. Choi, H.-W. Jang, and J.-L. Lee, Appl. Phys. Lett. **82**, 1233 (2003).

[9] Z. Mouffak, A. Bensaoula, and L. Trombetta, J. Appl. Phys. **95**, 727 (2004).

[10] C. Cheng and J. Si: Physica B **406**, 3098 (2011).

[11] K. Tang, W. Huang, and T. P. Chow, J. Electron. Mater. **38**, 523 (2009).

[12] Z. Yatabe, Y. Hori, S. Kim, and T. Hashizume, Appl. Phys. Express **6**, 016502 (2013).

[13] Y. Hori, C. Mizue, and T. Hashizume, Jpn. J. Appl. Phys. **49**, 080201 (2010).

[14] C. Mizue, Y. Hori, M. Miczek, and T. Hashizume, Jpn. J. Appl. Phys. **50**, 021001 (2011).

[15] S. Yang, Z. Tang, K.-Y. Wong, Y.-S. Lin, C. Liu, Y. Lu, S. Huang, and K. J. Chen, IEEE Electron Device Lett. **34**, 1497 (2013).

[16] M. Fagerlind, F. Allerstam, E. Ö. Sveinbjörnsson, N. Rorsman, A. Kakanakova-Georgieva, A. Lundskog, U. Forsberg, and E. Janzén, J. Appl. Phys. **108**, 014508 (2010).

[17] M. Ťapajna and J. Kuzmík, Appl. Phys. Lett. **100**, 113509 (2012).

[18] Z.-Q. Fang, D. C. Look, X.-L. Wang, J. Han, F. A. Khan, and I. Adesida, Appl. Phys. Lett. **82**, 1562 (2003).

[19] M. Miczek, C. Mizue, T. Hashizume, and B. Adamowicz, J. Appl. Phys. **103**, 104510 (2008).

[20] M. Miczek, B. Adamowicz, C. Mizue, and T. Hashizume, Jpn. J. Appl. Phys. **48**, 04C092 (2009).

[21] T. Hashizume, Proc. 9th International Conference on Advanced Semiconductor Devices and Microsystems (ASDAM 2012), 2012, p. 31.

[22] S. S. Mehari, E. Yalon, A. Gavrilov, D. Mistele, G. Bahir, M. Eizenberg, and D. Ritter, IEEE Trans. Electron Dev. **61**, 3558 (2014).

[23] S. Huang, Q. Jiang, S. Yang, Z. Tang, and K. J. Chen, IEEE Electron Device Lett. **34**, 193 (2013).

[24] T. Hashizume and H. Hasegawa, Appl. Surf. Sci. **234**, 387 (2004).